ADVANCED MATERIALS INTERFACES
Open Access
www.advmatinterfaces.de

Annealing-Free Ohmic Contacts to *n*-Type GaN via Hydrogen Plasma-Assisted Atomic Layer Deposition of Sub-Nanometer AlO_x

Maximilian Christis, Alex Henning, Johannes D. Bartl, Andreas Zeidler, Bernhard Rieger, Martin Stutzmann, and Ian D. Sharp**

A plasma-assisted atomic layer deposition (PE-ALD) process is reported for creating ohmic contacts to n-type GaN that combines native oxide reduction, near-surface doping, and encapsulation of GaN in a single processing step, thereby eliminating the need for both wet chemical etching of the native oxide before metallization and thermal annealing after contact formation. Repeated ALD cycling of trimethyl aluminum (TMA) and high-intensity hydrogen (H_2) plasma results in the deposition of a sub-nanometer-thin (≈8 Å) AlO_x layer via the partial transformation of the GaN surface oxide into AlO_x. Hydrogen plasma-induced nitrogen vacancies in the near-surface region of GaN serve as shallow donors, promoting efficient out-of-plane electrical transport. Subsequent metallization with a Ti/Al/Ti/Au stack results in low contact resistance, ohmic behavior, and smooth morphology without requiring annealing. This electrical contracting approach thus meets the thermal budget requirements for Si-based complementary metal–oxide–semiconductor structures and can facilitate the design and fabrication of advanced GaN-on-Si heterodevices.

1. Introduction

In addition to its widespread use in solid-state lighting applications, gallium nitride (GaN) has attracted increasing interest for its potential to replace or enhance Si-based complementary metal oxide semiconductor (CMOS) technology. In particular, the integration of high-performance GaN devices on CMOS platforms has enabled breakthroughs in advanced heterosystems for application in high-frequency telecommunications,[1] power switching,[2] and optoelectronics.[3] However, ensuring the stability of temperature-sensitive components in all fabrication steps becomes increasingly challenging as devices with more complex GaN- and CMOS-based structures are realized. Indeed, fabrication of ohmic contacts to GaN, often among the last production steps before encapsulation and backend processing, exceeds the temperature budget of essential structures in GaN-on-Si heterodevices when conventional contacting approaches (>700 °C) are used. For example, the AlGaN buffer layer in AlGaN/GaN high electron mobility transistors (HEMTs) is sensitive to performance-degrading oxidation at temperatures as low as 400 °C.[4] Combining surface passivation, which comes at the cost of larger negative threshold voltages, with intermediate-temperature (550 °C) contacting schemes yields acceptable performance characteristics.[5–8] Still, lower temperature approaches to contacting AlGaN/GaN structures with no or ultrathin passivation could further improve performance, as has been demonstrated for analogous InAlN devices.[9] Additionally, considering the thermal budget of CMOS structures (≈525 °C),[10] the high-temperature requirements of conventional GaN contacts forbid their fabrication after any backend processing has occurred, imposing a general limit on device design. Finally, Al tends to ball up at temperatures above its melting point (660 °C), meaning Ti/Al-based contacts exhibit a rough surface morphology after annealing,[11] which severely reduces adhesion when used as a metal interlayer in low-temperature wafer bonding.[12] These considerations highlight that low-temperature contacting approaches with competitive resistivities and smooth surface morphologies

M. Christis, A. Henning, J. D. Bartl, A. Zeidler, M. Stutzmann, I. D. Sharp
Walter Schottky Institute
Technical University of Munich
85748 Garching, Germany
E-mail: alex.henning@wsi.tum.de; sharp@wsi.tum.de

M. Christis, A. Henning, J. D. Bartl, A. Zeidler, M. Stutzmann, I. D. Sharp
Physics Department, TUM School of Natural Sciences
Technical University of Munich
85748 Garching, Germany

J. D. Bartl, B. Rieger
WACKER-Chair for Macromolecular Chemistry, Department of Chemistry, TUM School of Natural Sciences
Technical University of Munich
80333 München, Germany

The ORCID identification number(s) for the author(s) of this article can be found under https://doi.org/10.1002/admi.202300758

© 2023 The Authors. Advanced Materials Interfaces published by Wiley-VCH GmbH. This is an open access article under the terms of the Creative Commons Attribution License, which permits use, distribution and reproduction in any medium, provided the original work is properly cited.

DOI: 10.1002/admi.202300758

 © 2023 The Authors. Advanced Materials Interfaces published by Wiley-VCH GmbH

are needed to advance the design of novel GaN-on-Si heterodevices.

Low-impedance contacts to GaN have been a research subject since the early 1990s,[13,14] and contact resistivities below 10^{-6} Ω cm^2 are now readily achieved.[15] Greco et al.[15] have provided a detailed review of the role of different metal layers in ohmic contact formation and the various considerations for choosing an appropriate contact structure. In brief, most approaches to contacting *n*-type GaN rely on an annealed Ti/Al multilayer structure with a capping layer. Upon annealing, the thermodynamically driven interfacial reaction of Ti (Al) with GaN yields low work function TiN_x (AlN_x) compounds while generating N vacancies (v_N) within the GaN lattice.[16] Importantly, v_N act as shallow donors in GaN, resulting in heavily *n*-doped surface layers that reduce the space charge width and facilitate charge carrier tunneling. The optimal annealing temperature for such alloyed contacts is in the range of 650–850 °C.[15] However, for the reasons outlined above, research interest in non-alloyed contacts produced at lower processing temperatures has increased since the first GaN-on-Si heterodevices were conceived.

The first reported approaches for non-alloyed ohmic contacts to *n*-doped GaN[17,18] relied on the wet chemical etching of the native oxide before evaporation of a low-work function material. With contact resistivities below 10^{-4} Ω cm^2 on highly doped *n*-GaN substrates ($N_D \geq 10^{18}$ cm^{-3}), these contacts showed improved thermal stability and surface morphology compared to annealed contacts but did not match their low impedance and required harsh chemical etching steps. More recently, Wu et al.[19] reported a novel approach for achieving annealing-free ohmic contacts to *n*-GaN that relies on the passivation of the GaN surface using atomic layer deposition (ALD) of Al_2O_3. They hypothesized that the surface passivation reduces Fermi level pinning, lowering the Schottky barrier height between GaN and the low work function metal Yb (Φ_{Yb} = 2.6 eV). In contrast, Akazawa et al.[20] found that Fermi level pinning increases upon inserting a 1 nm thin Al_2O_3 interlayer at GaN/metal interfaces. Additional insight into the nature of this interface comes from the observation that thermal ALD of Al_2O_3 monotonically reduces GaN surface band bending with increasing Al_2O_3 thickness.[21,22] This behavior could be explained by a charge compensation mechanism involving electron donor states in bulk Al_2O_3 possessing energy levels between the conduction band minima of GaN and Al_2O_3.[21,22] For the GaN/Al_2O_3/Yb contacts reported by Wu et al.,[19] the contact resistivity increased with Al_2O_3 layer thickness, suggesting that the benefits of increasing charge compensation are outweighed by the thicker tunneling barrier imposed by Al_2O_3. Indeed, the optimal Al_2O_3 layer thickness may be lower than the minimum of 1 nm deposited by Wu et al.[19] However, continuous ultrathin films are difficult to achieve via thermal ALD of Al_2O_3. In particular, during film nucleation, adsorption energetics, precursor steric effects, and substrate surface inhomogeneities prevent complete saturation of the available surface binding sites.[23] For ultrathin films down to the monolayer limit, this means incomplete coverage of the substrate surface, interface roughening, and inhomogeneous junction energetics. Thus, an approach to grow conformal ultrathin Al_2O_3 films can potentially improve metal–insulator–semiconductor (MIS) contacts by minimizing the tunneling barrier while maintaining the desired interfacial characteristics introduced by the dielectric.

In recent work,[24] we investigated the surface chemistry of an ALD process based on repeated cycling of trimethyl aluminum (TMA) and H_2 plasma (HP) exposure. Using a low HP power of 100 W, we demonstrated that the GaN surface can be encapsulated with an ultimately thin AlO_x monolayer via solid-state conversion of the GaN native oxide into AlO_x. The low HP power enabled closed monolayer growth by stripping the remaining methyl ligands from the adsorbed TMA precursor in a ligand exchange reaction. The reaction self-terminates upon exhaustion of available surface binding sites, enabling closed films down to the monolayer limit. Here, we report an analogous HP/TMA ALD process that has been adapted to promote the formation of low resistance ohmic contacts to *n*-type GaN. To achieve this, the HP power was increased to 300 W, resulting in a higher electron excitation temperature of (10.2 ± 2.3) × 10^3 K at the sample. This allows stronger interactions between reactive gas species and the near-surface region of the semiconductor, which alters the chemical composition of the interface during the self-limiting growth of a continuous sub-nanometer thin AlO_x overlayer. Using in situ spectroscopic ellipsometry (SE) combined with ex situ X-ray photoelectron spectroscopy (XPS), we find that the oxygen content in the native GaO_x overlayer decreases with the ALD cycle number, resulting in complete consumption of the oxygen after 200 ALD cycles. A fraction of this oxygen is incorporated in the AlO_x overlayer, whose growth self-terminates at the ultrathin limit (<1 nm) within the window of 12–20 cycles. In addition, the HP generates shallow donor states in the form of v_N in the near-surface region of GaN. The resulting interface exhibits significantly reduced surface band bending and contact resistivity compared to the bare GaN surface. Systematic characterization of the barrier height across a series of metals reveals increased Fermi level pinning (FLP) compared to the bare GaN, consistent with the presence of incorporated defects arising from HP interaction with the solid during ALD. Importantly, contacting this modified GaN/AlO_x interface with a Ti/Al/Ti/Au metal stack yields low contact resistivities of (2.8 ± 0.4) × 10^{-4} Ω cm^2 even before thermal annealing. This value is comparable to state-of-the-art annealing-free contacts,[17–19] while eliminating the need for wet chemical surface pre-treatments and rare metals such as Yb.[19] Thus, engineering of GaN interfaces via HP-based ALD of ultrathin AlO_x layers provides a viable approach to high-quality etching- and annealing-free electrical contacts to *n*-type GaN, of relevance for GaN-on-Si heterodevices where the degradation of temperature-sensitive components must be avoided. Furthermore, by encapsulating favorable surface modifications in a near-transparent and stable AlO_x layer, the proposed ALD treatment could improve existing specialized contacting schemes, such as transparent indium tin oxide (ITO) contacts relevant to LED applications.[25] Finally, since the presented contacting approach does not rely on the alloying properties of the utilized metal stack, an Au-free contact for CMOS compatibility with minimal work function could be realized.

2. Results and Discussion

2.1. GaN Native Oxide Reduction and AlO_x Formation

The effect of a high-power (300 W) HP-assisted ALD process on the chemical composition of the GaN surface was first

© 2023 The Authors. Advanced Materials Interfaces published by Wiley-VCH GmbH

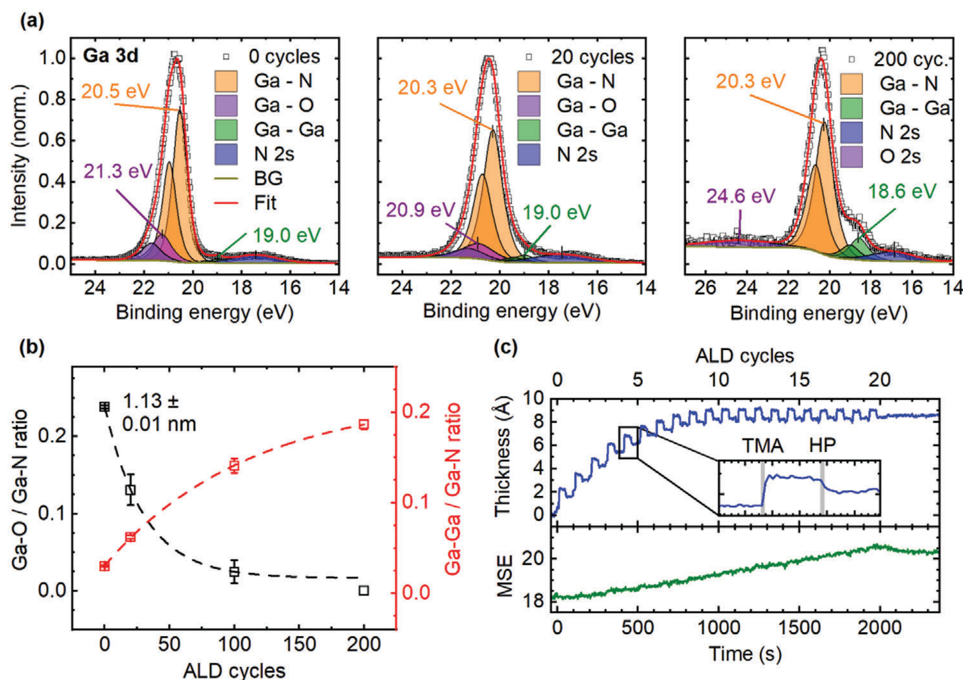

Figure 1. Chemical composition of the native GaN/GaO_x surface before and after HP/TMA exposure. a) Ga 3d core level spectrum before (left) and after 20 (middle) and 200 (right) HP/TMA treatment cycles. b) Ga–O/Ga–N (black) and Ga–Ga/Ga–N (red) chemical bonding ratios extracted from the Ga 3d core level spectra. The calculated GaO_x thickness for the bare sample is written next to the respective data point. c) Real-time in situ spectroscopic ellipsometry monitoring of the ALD process during 20 cycles of HP/TMA exposure (AlO_x overlayer thickness (blue), mean square error of fit (green)). The inset shows the fifth process cycle in detail, where grey bars indicate the times of TMA and HP exposure.

investigated via XPS measurements. **Figure 1a** shows Ga 3d core level spectra of solvent-cleaned GaN before the process, as well as after 20 and 200 cycles of HP and TMA exposure. The spectra were deconvoluted into components corresponding to Ga–N, Ga–O, and Ga^0 (denoted as Ga–Ga) states, along with the neighboring N 2s satellite. Each Ga 3d component was fitted with a fixed spin–orbit splitting of 0.43 eV,[26,27] area ratio of 3:2, and equal full width at half maximum (FWHM). The Ga–O component associated with the native oxide is chemically shifted by $+0.8 \pm 0.1$ eV with respect to the main Ga–N component from the substrate for all samples, consistent with our previous report.[24] Following sequential exposure of the surface to 300 W HP/TMA cycles, a decrease in Ga–O/Ga–N component intensity ratio is observed, indicating the removal of native oxide. An increase in exposure cycles from 20 to 200 led to a more pronounced reduction of this Ga–O component. Accompanying this change, an increase in the relative intensity of the Ga–Ga component at lower binding energy was also observed. As discussed below, this is attributed to both the reduction of GaO_x and the formation of v_N within the GaN lattice.

The qualitative changes described above are quantified in Figure 1b, which shows both the Ga–O/Ga–N and the Ga–Ga/Ga–N component intensity ratios as a function of the number of HP/TMA cycles. A corresponding effective thickness of 1.13 ± 0.01 nm for the GaO_x overlayer of bare GaN was determined according to Equation S1 (see Section S1.1, Supporting Information).[28] The Ga–O/Ga–N intensity ratio decreases asymptotically with cycle number, with no Ga–O component detectable after 200 cycles, indicating that the surface becomes completely depleted of oxygen. Such behavior was not observed for our previously reported analogous lower power (100 W) HP process. In that work, GaO_x consumption was limited to the ligand-exchange reaction of surface Ga–OH groups to form Ga–O–Al moieties upon TMA adsorption, resulting in encapsulation of the surface with an ultimately thin AlO_x monolayer (3 Å). In the present work, we find that using a higher HP power (300 W) leads to stronger chemical interactions that extend below the interface, resulting in the consumption of oxygen from within the complete native oxide layer. The influence of the HP on the near-surface region is further evidenced by the increasing Ga–Ga/Ga–N component intensity ratio (Figure 1b, red curve), which is discussed below and indicates the chemical modification of the underlying GaN.

The formation of an AlO_x overlayer on the substrate via the HP/TMA process is confirmed by XPS measurements of the Al 2p region (Figure S1, Section S1.2, Supporting Information). After 20 treatment cycles, a single component at 75.2 eV is present that can be assigned to Al─O bonding. For ≥100 ALD cycles, where complete depletion of oxygen from the native oxide layer is observed, an additional XPS component appears at 74.1 eV. This lower binding energy component is consistent with the formation of AlC_x species, with the TMA ligands likely serving as the carbon source. Such AlC_x formation was also observed for the lower power (100 W) HP process,[24] and was found to be associated with the exhaustion of Ga–OH surface binding sites. In the present work, we find that carbide formation negatively impacts the electronic quality of the interface and interferes with ohmic contact formation (Figure S3, Section S2, Supporting

© 2023 The Authors. Advanced Materials Interfaces published by Wiley-VCH GmbH

Information). Furthermore, angle-resolved XPS measurements suggest that such extended HP/TMA cycling, with near-complete consumption of the GaO_x, can lead to the formation of metallic Ga at the interface between GaN and AlO_x (Figure S4, Supporting Information). Therefore, we focus our attention for the remainder of this work on samples generated with 20 ALD cycles, where the native GaO_x is partially converted to AlO_x and no detectable traces of AlC_x are present.

To determine the thickness of the deposited AlO_x layer after 20 HP/TMA cycles, we employed in situ spectroscopic ellipsometry. The resulting data were analyzed using a Cauchy dispersion model with the optical parameters of alumina (see Experimental Section; Section S4, Supporting Information). Figure 1c shows the thickness extracted from SE data, along with the mean square error of the fit, as a function of time during deposition. The growth per cycle (GPC), defined as the increase in thickness for a single ALD cycle, is positive and decreases during the first 12 cycles. This behavior is similar to that of the previously reported low-power HP/TMA process, in which a decrease of the GPC was found to be driven by consumption of available surface Ga–OH since no gas phase oxidant was introduced into the system. In that case, growth saturated after eight cycles at an AlO_x thickness of 2.8 ± 0.1 Å, corresponding to the single monolayer limit. For the higher power HP process reported here, a comparatively larger self-limiting AlO_x thickness of 8.0 ± 0.1 Å is observed. This finding is consistent with the observed depletion of oxygen from the complete native GaO_x layer, which serves as a solid-state source of oxygen for the growing AlO_x layer.

We note that oxygen incorporation into the growing AlO_x from the gas phase can be excluded since no decay of the TMA adlayer thickness was observed during in situ SE measurements on a timescale of hours after a single precursor pulse in the absence of additional ALD steps (Figure S6, Section S5, Supporting Information). Considering that any gas phase oxidants, such as those arising from trace contamination in the chamber, would rapidly react with TMA and lead to a detectable loss of methyl ligands, it is possible to conclude that such processes have a negligible influence on AlO_x film formation. Instead, the oxygen necessary for forming the AlO_x layer must stem from a solid-state exchange with the underlying GaO_x. This is consistent with our prior findings,[24] as well as the observation of GaO_x reduction concurrent with AlO_x growth.

To better understand oxygen transfer from the GaO_x to the AlO_x layer, we highlight four consecutive mechanistic steps: i) in-diffusion of reactive H radicals/ions, ii) breaking of Ga–O bonds, iii) out-diffusion of mobile O species through the GaO_x and AlO_x overlayers, and iv) formation of Al─O bonds. Given the highly reductive potential of the H_2 plasma species,[29] as well as the significant reactivity of TMA,[23] steps (ii) and (iv) are assumed to occur quickly and are thus unlikely to limit the rate of AlO_x film formation. We therefore consider the kinetics associated with diffusive steps (i) and (iii) in greater detail. Regarding step (i), we note that the direct interaction of energetic H_2 plasmas with β-Ga_2O_3 layers at moderate temperatures has been previously investigated and revealed large diffusion lengths of several hundred nm, even at moderate temperatures comparable to those used here.[30,31] Furthermore, large penetration depths of remote H_2 plasma have been demonstrated on other oxide and semiconductor films, such as GaN,[32] ZnO,[33] and SiO_2.[34] Thus, it is considered unlikely that in-diffusion of reactive hydrogen species through the 1 nm thick native GaO_x overlayer represents a limiting step for eventual oxygen exchange. Based on these considerations, it is reasonable to expect that the out-diffusion of mobile oxide species in step (iii) plays a defining role in GaO_x reduction and AlO_x formation.

The driving force for oxygen migration is its propensity to react with undercoordinated O─Al* surface sites generated during H_2 plasma exposure, during which the methyl ligands of chemisorbed TMA are reduced to methane that leaves in the gas phase. However, the reaction is likely limited by the slow kinetics of oxygen transport in GaO_x and AlO_x. Indeed, thermal activation energies for oxygen self-diffusion in GaO_x are large and range from 0.8 eV in the amorphous phase[35] to 3.2 eV for crystalline β-Ga_2O_3.[36] A similar thermal activation energy of 1.2 eV[37,38] has been reported for oxygen self-diffusion in amorphous Al_2O_3. On the other hand, oxygen diffusion lengths associated with this process are extremely small, on the order of 1 nm. Thus, the observed decrease of GPC and eventual saturation of AlO_x thickness with repeated cycling (Figure 1d) can be understood by considering that only oxygen that reaches the sample surface will be available for reaction with O─Al* sites on the surface, that the oxygen from the GaO_x layer is progressively consumed with repeated cycling, and that the diffusion lengths increase as the AlO_x layer forms.

We note that while the native oxide of GaN served as the oxygen source for the ALD AlO_x growth reported here, other types of surface oxides may be considered in the future to further tune the interfacial properties. For example, controlled oxidation of pristine GaN substrates under ultrahigh vacuum conditions can yield crystalline gallium oxide with a thickness controllable down to the monolayer limit,[39] which could be engineered as an ideal starting layer for subsequent ALD of AlO_x in the future. However, differing oxygen diffusion coefficients and lengths through such layers are likely to impact the kinetics of the oxide interconversion process.

2.2. Nitrogen Vacancy (v_N) Generation

Nitrogen vacancies in GaN exhibit negative formation energies under most growth and processing conditions, except for extreme N-rich environments, and act as shallow *n*-type dopants that can significantly influence the electronic properties of GaN.[40] As described above, conventional approaches to contacting *n*-type GaN rely on v_N generation by high-temperature annealing of a Ti overlayer to create a highly *n*-doped surface. In the present work, the possibility of HP-induced generation of v_N, as well as its influence on interface energetics and contact resistivity, was investigated. To this end, the atomic concentration ratio [N]/[Ga] in the GaN surface region was derived from the ratio of the N-Ga components of the N 1s and Ga 3d core level regions according to Equation S3a–d (Section S1.3, Supporting Information). **Figure 2** shows the [N]/[Ga] ratio for a bare GaN sample compared to a control sample subjected to 120 s of a continuous 300 W HP, as well as a sample subjected to 20 cycles of the 300 W HP/TMA ALD treatment. The bare GaN sample exhibits a [N]/[Ga] ratio of 0.70 ± 0.09, consistent with a prior report on GaN grown by hybrid vapor phase epitaxy (HVPE).[41] In contrast, the sample treated with a continuous HP shows a

© 2023 The Authors. Advanced Materials Interfaces published by Wiley-VCH GmbH

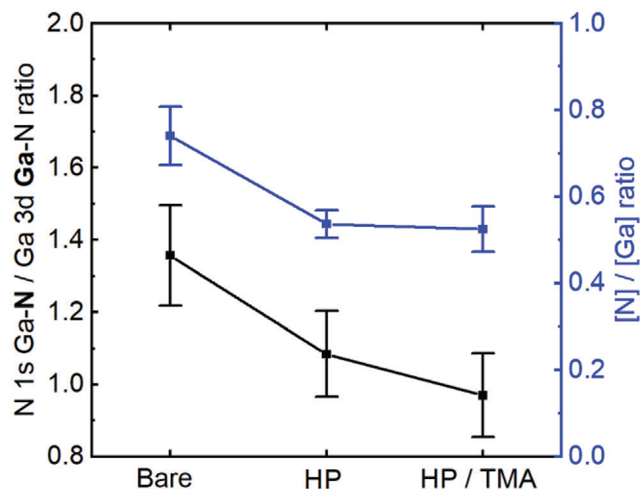

Figure 2. Peak area ratio (black) of the N 1s Ga–**N** and the Ga 3d **Ga**–N components of the XPS spectra of *n*-type GaN before HP exposure ("Bare"), after 120 s of continuous 300 W HP exposure ("HP"), and after 20 HP/TMA cycles ("HP/TMA"). Also shown is the attenuation-corrected atomic [N]/[Ga] ratio (blue).

significantly lower ratio of 0.54 ± 0.03. Importantly, a similarly reduced ratio of 0.53 ± 0.05 is obtained for the HP/TMA treated sample. The decreased [N]/[Ga] ratios reveal the loss of lattice N from the near-surface region of GaN and provide a strong indication for the formation of v_N. This increase in v_N concentration is expected to increase the *n*-type doping of the near-surface region and can partially explain the beneficial effect of the HP/TMA treatment on contact resistivity, as discussed below.

2.3. Surface Band Bending and Schottky Barrier Height

The compositional changes of the *n*-type GaN/GaO_x surface introduced by repetitive cycles of HP/TMA exposure significantly impact the surface potential. **Figure** 3a shows contact potential difference (CPD) measurements performed before and after the HP/TMA ALD process. In particular, the fast surface photovoltage (SPV) response generated by illumination with above-bandgap (340 nm) light is decreased from 0.5 to 0.2 V. The slow increase of the CPD signal during illumination for bare GaN is ascribed to photo-induced surface oxide growth.[42] Importantly, the increased stability of the SPV signal for the HP/TMA treated sample indicates chemical passivation of the interface under sustained UV illumination due to the presence of AlO_x at the surface. As is evident from Figure 3b, the SPV of the HP/TMA-exposed sample is consistently decreased across a broad range of illumination intensities, indicating reduced surface band bending. In our previous work with the low power (100 W) HP process,[24] no such reduction in band bending was observed. This suggests that chemical changes in the interface induced by the higher plasma power introduce electronically active defects in the near-surface region. Such defects could also contribute to the much slower relaxation kinetics observed after the cessation of illumination for the HP/TMA-treated sample, with charge separation and trapping near the interface, combined with the wide bandgap semiconductor GaN, leading to long lifetimes of trapped carriers.

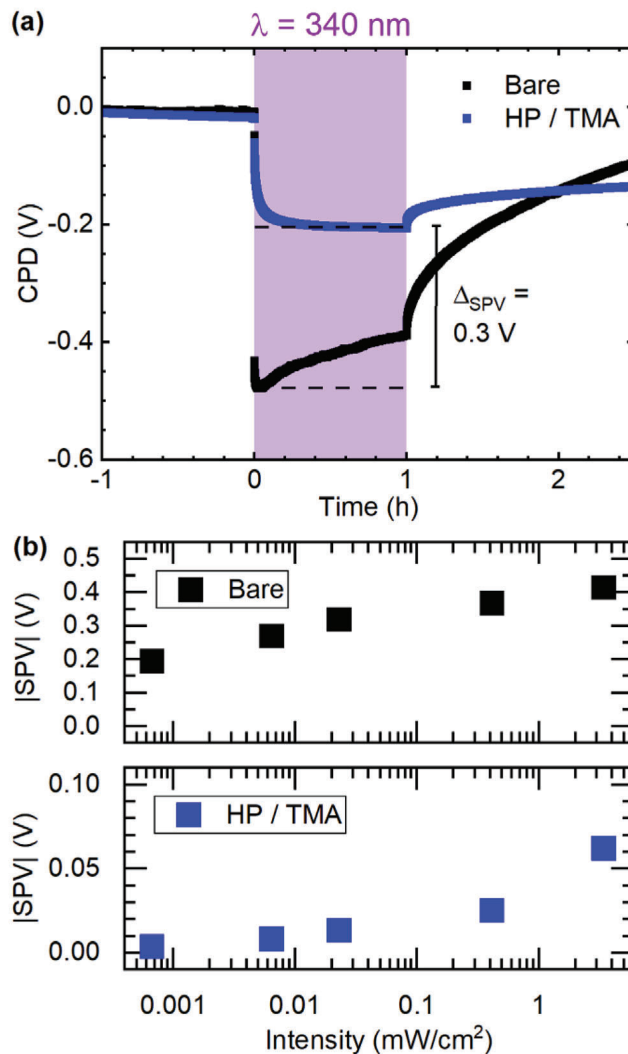

Figure 3. Interface potential responses of GaN surfaces before and after the AlO_x deposition. a) Contact potential difference and surface photovoltage measurements of *n*-type GaN before (black) and after (blue) 20 cycles of sequential HP/TMA exposure. The period of illumination with above-bandgap radiation (λ = 340 nm) is marked in violet. b) Fast SPV values (measured 40 s after switching the illumination on) recorded for the same samples as a function of illumination intensity.

However, due to the complex nature of the interface, it is not yet possible to unambiguously assign the specific defect type responsible for this behavior. While the suggested increase of v_N in the near-surface region could yield this reduced SPV, defects introduced in the GaO_x during its chemical reduction by the HP or in the disordered AlO_x formed on its surface could also contribute to the observed behavior.

For Al_2O_3 layers grown via thermal ALD on GaN using H_2O as the oxidant, Gong et al.[21] observed a band bending reduction that increased with Al_2O_3 thickness. As a possible mechanism, they suggested that electron transfer from negatively charged defect states in Al_2O_3 partially compensates for the electron depletion in the GaN space charge region. This mechanism, initially hypothesized by Esposto et al.,[22] requires the presence of

© 2023 The Authors. Advanced Materials Interfaces published by Wiley-VCH GmbH

electron donor states in Al_2O_3 with energy levels higher than those of the GaN surface defect states. Importantly, interstitial hydrogen has been proposed as the dominant electronic defect in amorphous Al_2O_3,[43] acting as a shallow donor state.[44] Thus, a large concentration of interstitial H in the AlO_x overlayer after H_2 plasma treatment could explain the reduced SPV. On the other hand, similar changes in band bending were not observed from HP processes with lower power despite there also being an ample source of atomic hydrogen. Instead, the primary difference between the low and high-power HP processes is associated with chemical changes below the surface. This line of reasoning suggests that electronically active defects in the oxygen-deficient GaO_x or v_N in the GaN, both of which are generated during the 300 W HP process, play an important role in defining the interface band energy profile.

To investigate the effect of reduced surface band bending and increased v_N concentration on out-of-plane electrical transport properties, Schottky contacts were fabricated using Ti, Cr, Au, and Pt. Schottky barriers were determined both for the bare GaN/metal interfaces and GaN/AlO_x/metal interfaces via current density–voltage (J–V) measurements (Section S6, Supporting Information). The J–V characteristics of Schottky diodes with the high work function metals Pt and Au are shown in **Figure** 4a,b. A comparison of the transport characteristics of the coplanar contacts reveals a significant current increase for the *n*-type GaN/AlO_x/metal structures generated by the HP/TMA process compared to the bare GaN/metal structures. This increased current is particularly pronounced in the reverse bias direction and indicates a significant reduction of the Schottky barrier induced by our ALD process. Considering the ultrathin nature of the introduced AlO_x interlayer, facile tunneling across the dielectric is possible, and the reduced Schottky barrier height plays a dominant role in reducing the overall junction impedance.

The extent of Fermi level pinning (FLP) for both types of samples was quantified by extracting the surface index, *S*, from linear fits of the Schottky barrier, ϕ_M, as a function of the metal work function, ϕ_M, according to:[45]

$$S = \frac{\delta\phi_B}{\delta\phi_M} \quad (1)$$

Here, the limiting case of $S = 1$ describes an ideal Schottky contact in the absence of surface states, while the other limit of $S = 0$ describes the Bardeen limit of complete FLP arising due to the presence of high concentrations of interface states. Figure 4c shows the measured Schottky barriers of bare GaN/metal interfaces and GaN/AlO_x/metal interfaces as a function of the metal work function. For bare GaN, the barrier height moderately depends on the metal work function, with $S = 0.53 \pm 0.07$. This finding is consistent with previous reports for HVPE-grown *n*-type GaN of similar doping concentration, which have yielded values between 0.23 and 0.49.[46,47] Such a significant spread is common and arises from differences in material quality, surface treatments, and the method of contact metal deposition.[47] Excluding the effects of reconstruction and chemical modification of the semiconductor surface, the metal-induced gap states (MIGS) model for Schottky barrier formation predicts a theoretical value of $S = 0.31$ for GaN/metal interfaces.[48]

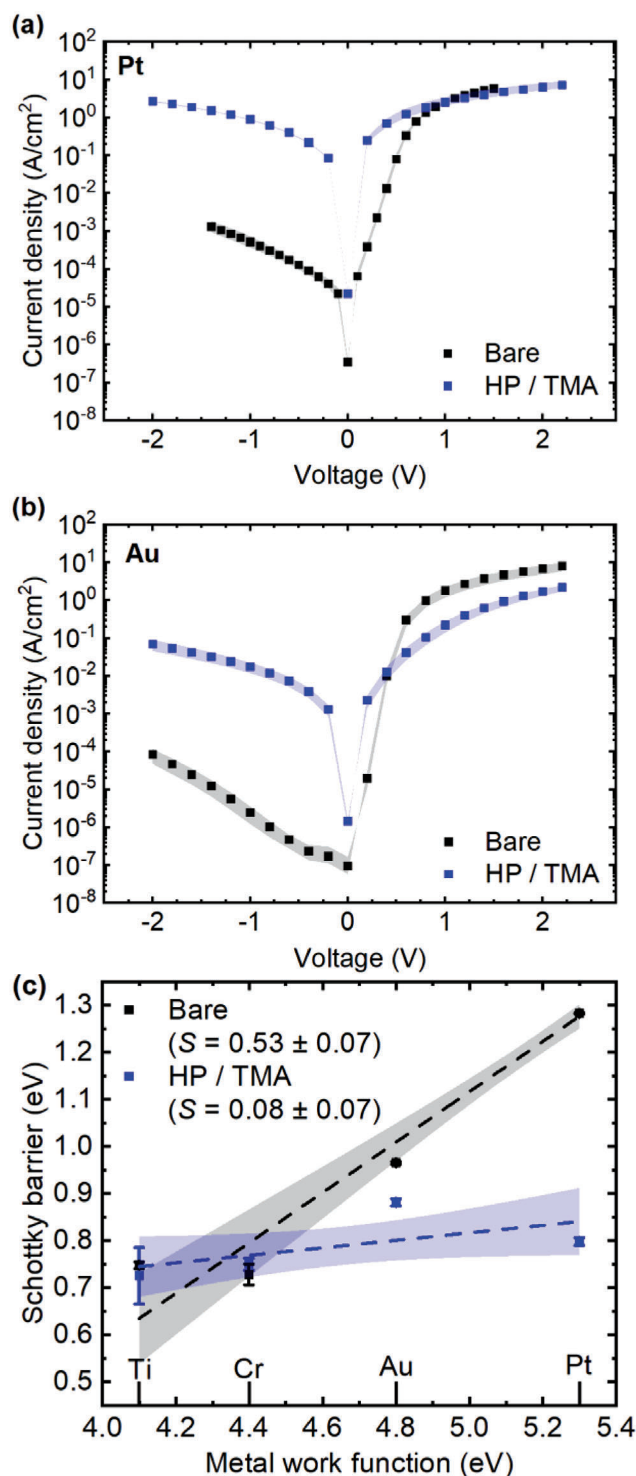

Figure 4. J–V characteristics of a) Pt and b) Au Schottky contacts to *n*-type bare GaN (black) and GaN exposed to 20 HP/TMA ALD cycles (blue). Semitransparent bands indicate the spread (minimum to maximum) between currents measured for different contacts on the same substrate. c) Schottky barrier heights for *n*-type GaN contacted with different metals possessing a range of work functions (Ti: 4.1 eV, Cr: 4.4 eV, Au: 4.8 eV, Pt: 5.3 eV). Semitransparent bands indicate 65% confidence intervals for the linear fits to the experimentally determined barrier heights (dashed lines).

© 2023 The Authors. Advanced Materials Interfaces published by Wiley-VCH GmbH

For MIS contacts, such as the GaN/AlO_x/metal structure investigated here, the MIGS model qualitatively predicts an increase of S since the insulating interlayer should attenuate the exponential tail of electron wave functions extending from the metal into the semiconductor. Indeed, the penetration depth of MIGS is typically in the range of 1.5–4 Å,[49] which is well below the measured AlO_x thickness of 8 Å. Such a Fermi level depinning effect has been experimentally demonstrated for a thin MgO layer inserted at the *n*-type GaN/metal interface.[46] However, for a 1 nm thin Al_2O_3 interlayer grown by thermal ALD, slightly increased FLP (decreased S) was previously observed.[20] Similarly, the HP/TMA ALD process investigated here results in increased FLP ($S = 0.08 \pm 0.07$). This near-total Fermi level pinning cannot be described by the MIGS model but can instead be ascribed to high concentrations of defects with localized energy distributions at the interface.[50] This assignment is consistent with the substantial chemical modification to the interface described above. Interestingly, the HP/TMA treatment leads to a general reduction of the Schottky barrier for the investigated metal contacts. In contrast, an increased average Schottky barrier height by 0.07 eV was previously observed upon insertion of a 1 nm thin thermal ALD Al_2O_3 interlayer at the *n*-type GaN/metal interface,[20] suggesting that the observed barrier lowering is a consequence of the HP-based process. In addition, Schottky contacts to the HP/TMA treated samples exhibit larger ideality factors than the bare GaN samples (Figure S7, Supporting Information). Generally, Schottky contacts can display increased ideality factors when the potential barrier height is laterally distributed rather than constant across the Schottky contact.[51] Consistent with the line of reasoning presented above, electronically active defects in the oxygen-deficient GaO_x or v_N in the GaN generated by the 300 W HP treatment may lower the Schottky barrier locally, providing favorable pathways for charge transport across the Schottky contact and broadening the overall distribution of barrier heights.

2.4. Reduced Contact Resistivity and Ohmic Contact Formation

Considering the significant Schottky barrier height reduction observed above, we sought to investigate how treatment of the *n*-type GaN surface with 20 HP/TMA cycles impacts interfacial electron transport using low work function contacts based on Ti. To this end, Ti/Al/Ti/Au (20/80/10/90 nm) top contacts were fabricated on an ALD-treated sample. As described above, similar metal stacks are commonly used for manufacturing electrical contacts to *n*-type GaN but require high temperature (T > 650 °C) annealing to achieve ohmic transport characteristics. **Figure 5a** compares the J–V characteristics of these as-deposited contacts applied to bare GaN surfaces and GaN/AlO_x surfaces generated via the HP/TMA process, both without annealing. While a bare GaN reference with unannealed Ti/Al/Ti/Au contacts showed the J–V characteristics of two Schottky diodes in back-to-back configuration and a negligible current density, the ALD treated sample exhibits ohmic characteristics over the complete voltage range of ±2.0 V. Remarkably, transfer length method (TLM) measurements of the annealing-free contacts (Section S7, Supporting Information) yield a contact resistivity of $(2.8 \pm 0.4) \times 10^{-4}$ Ω cm^2 which is comparable to state-of-the-art annealing-free contacts to

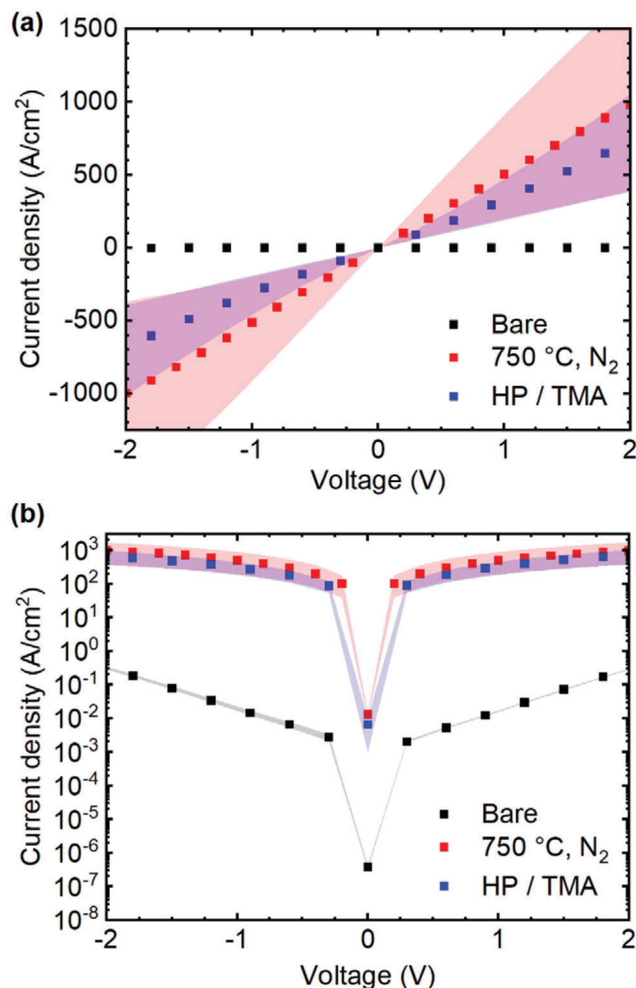

Figure 5. J–V characteristics in a) linear and b) logarithmic scale of bare *n*-type GaN with unannealed Ti/Al/Ti/Au (20/80/10/90 nm) contacts (black), bare *n*-type GaN with conventional Ti/Al/Ti/Au (20/80/10/90 nm) contacts annealed for 300 s at 750 °C in N_2 atmosphere (red), and *n*-type GaN sequentially exposed to 20 HP/TMA cycles with unannealed Ti/Al/Ti/Au contacts (blue). Transparent bands indicate the spread (minimum to maximum) across the recorded J–V data.

n-type GaN.[17–19] As expected, the non-alloyed contacts exhibit a smooth surface morphology with a root mean square (RMS) roughness of 1.16 ± 0.08 nm (Section S8, Supporting Information).

The resistivity of contacts prepared by the HP/TMA process without additional annealing compares favorably to measurements on benchmark annealed contacts produced on a bare GaN surface with Ti/Al/Ti/Au (20/80/10/90 nm) contacts activated by annealing at 750 °C in N_2 atmosphere for 300 s (Figure 5). For these annealed contacts, it is important to note that wet chemical stripping of the native oxide is essential to ensure that the thermal reaction of Ti with GaN occurs to generate v_N and, thus, a highly-doped interface.[15] By contrast, chemical etching is not required for annealing-free ohmic contact formation via the ALD process reported here. Indeed, nominally identical contact resistances were obtained for Ti/Al/Ti/Au contacts applied to HP/TMA treated surfaces, regardless of whether an HCl oxide

© 2023 The Authors. Advanced Materials Interfaces published by Wiley-VCH GmbH

etch was applied prior to ALD (Figure S8, Supporting Information). Consistent with the XPS measurements described above, this indicates that interaction of the HP with the underlying GaN generates the requisite v_N and corresponding highly doped surface region required for low impedance ohmic contact formation without the need for thermal annealing. As such, the reported contact fabrication scheme utilizing HP-assisted ALD can eliminate both the high-temperature annealing and wet-chemical etching steps that are needed for traditional ohmic contacts but can be problematic for the fabrication of integrated GaN-based devices. While a Ti/Al/Ti/Au contact stack was used here for direct comparison between annealed and non-annealed contacts, we expect that such ohmic behavior should be possible with a range of other low workfunction metal contacts, since there is no requirement for interfacial reaction of Ti (Al) to form TiN_x (AlN_x) and v_N. However, it is noted that this contact fabrication scheme can likely not be applied to *p*-type GaN since H is known to passivate the Mg defects most commonly used for *p*-type doping.[52]

3. Conclusion

In summary, we have presented an oxidant-free plasma-enhanced ALD process using TMA and 300 W H_2 plasma to fabricate sub-nanometer thin AlO_x films on GaN. The ALD treatment leads to beneficial modifications to the composition of the GaN surface, introducing N vacancies into the near-surface region and reducing the native GaO_x layer, thereby enabling the fabrication of ohmic contacts to the *n*-type semiconductor without the need for high-temperature annealing. The extent of native oxide consumption can be controlled via the number of ALD cycles, with complete oxygen depletion of the native oxide obtained after 200 cycles. However, saturated AlO_x film thicknesses of just 8 Å are obtained after a maximum of 20 HP/TMA cycles, while Al carbide formation is suppressed. The compositional changes at the interface induced by the 20-cycle HP/TMA ALD process significantly reduced surface band bending. Furthermore, evaluation of Schottky contacts produced on these surfaces revealed increased Fermi level pinning but reduced Schottky barrier heights for GaN/AlO_x/metal compared to GaN/metal interfaces. Taking advantage of these modified interface properties, we have fabricated Ti/Al/Ti/Au (20/80/10/90 nm) contacts to TMA/H_2 plasma treated *n*-GaN, which exhibited ohmic J–V characteristics with a contact resistivity as low as $(2.8 \pm 0.4) \times 10^{-4}$ Ω cm^2 even in the absence of annealing or surface chemical pretreatments, while also preserving a smooth surface morphology. This contact resistivity is comparable to the lowest values reported to date for completely annealing-free contacts (including those subjected to pre-deposition annealing[18]) to *n*-type GaN with similar doping concentrations.[17,19] Indeed, we find that the HP-based ALD process induces chemical changes to the GaN interface similar to those occurring during traditional high-temperature annealing for activation of Ti-based contacts on *n*-type GaN. While considerable opportunity remains for optimizing annealing-free contacts on GaN using this HP-based ALD surface treatment, our work provides a new route to low impedance and annealing-free electrical contacts to GaN, which is of key importance for the development of future GaN devices integrated with Si CMOS-technology.

4. Experimental Section

GaN Substrates: Single-side polished *n*-type (0001) Ga-polar GaN templates (4.5 ± 0.5 µm thick, Si-doped with nominal carrier concentration ≈2.0×10^{18} cm^{-3}, threading dislocation density < 5×10^8cm^{-2}, resistivity < 0.01 Ω cm at 300 K) grown by HVPE on 430 ± 25 µm thick sapphire wafers were obtained from MSE Supplies LLC (Arizona, USA). In-house Hall effect measurements confirmed the carrier concentration of 2.0×10^{18} cm^{-3}. The wafers were cut into 1 × 1 cm^2 pieces and cleaned by successive sonication in acetone, isopropanol, and deionized water for 10 min, respectively. The samples were stored in an N_2 dry box before further processing. To test for native oxide growth during the storage period, some samples were etched in a concentrated HCl (37%) solution. The post-etch native oxide thickness ranged between 1.0 and 1.2 nm, as determined via XPS (see Section S1.1, Supporting Information). These values agreed with the native oxide thickness measured on an as-received sample after solvent-cleaning and mild in situ Ar cluster sputtering (0.93 ± 0.14 nm), as well as on a sample measured after 1 month of storage (1.0 ± 0.2 nm). Therefore, the influence of the native oxide growth on the electrical performance of the annealing-free contacts to ALD-treated GaN was considered negligible within the given storage period. Notably, a wet chemical etch was not necessary to achieve desirable electrical properties of the fabricated annealing-free contacts. An HCl etch prior to further processing was therefore only conducted where explicitly stated.

Atomic Layer Deposition (ALD): Surface treatments of GaN substrates with TMA and HP or only HP was conducted in a hot-wall plasma-enhanced atomic layer deposition reactor (Fiji G2, Veeco CNT) in continuous flow mode. Before these processes, an in situ HP pretreatment (2 cycles, 3 s, 100 W, 0.027 mbar, 200 °C) was conducted to remove spurious carbon and, thus, improve the homogeneity of the ALD film nucleation[53] AlO_x films were grown by exposure to a TMA precursor (electronic grade, 99.999%, STREM Chemicals) in the first half-cycle and HP (99.9999%, Linde) in the second half-cycle. Each ALD cycle followed the sequence: 0.08 s TMA dose, 30 s Ar purge, 8 s H_2 purge, 3 s HP, 30 s Ar purge. During TMA exposure, Ar (99.9999%, Linde) was used as a carrier gas (p ≈ 0.12 mbar), with the turbo pump being isolated from the reactor. During the second half-cycle, H_2 was supplied at a base pressure of 0.027 mbar with an active turbo pump. HP was generated in a sapphire tube with an inductively coupled plasma source operating with a radio frequency (RF) bias of 13.64 MHz and a power of 300 W, resulting in an electron excitation temperature of $(10.2 \pm 2.3) \times 10^3$ K at the sample, as characterized by optical emission spectroscopy (Section S9, Supporting Information). The temperatures of the reactor walls and chuck were maintained at 200°C.

Spectroscopic Ellipsometry (SE): AlO_x growth on the GaN substrates during ALD was monitored with an in situ spectroscopic ellipsometer (J.A. Woollam, M-2000), as described in a previous report.[24] The SE spectra, obtained with an integration time of 3 s in a wavelength range between 210 and 830 nm, were fitted with a multilayer model in the least mean square approach (see Section S4, Supporting Information). The sapphire substrate was modeled using a Cauchy dispersion model with Al_2O_3 material parameters from the Woollam database (CompleteEASE, ver. 6.53, J.A. Woollam). For the GaN layer, a general oscillator model was used.[54] The optical constants and thickness of the native GaO_x layer were approximated directly before ALD with a generic oxide layer model adapted from the Woollam database and were kept constant during growth. Finally, AlO_x growth was modeled as a second Cauchy dispersion layer, with optical parameters for ALD alumina taken from our previous report.[24] Since this model assumes an Al_2O_3 stoichiometry for the grown AlO_x overlayer and does not account for structural changes in the GaO_x and GaN layers, an increasing error in the obtained AlO_x thickness is expected with an increasing number of ALD cycles. Nevertheless, the thickness obtained by SE after 20 ALD cycles agreed with XPS measurements.

Electrical Contacts and Characterization: Electrical contacts to the GaN and GaN/AlO_x samples were realized as Ti/Al/Ti/Au (20/80/10/90 nm) metal stacks deposited via electron-beam evaporation at pressures < 3×10^{-6} mbar. Low evaporation rates of 1 Å s^{-1} for Ti and 2 Å s^{-1} for Al and Au were chosen to prevent damage to the underlying layers during evaporation. For Fermi level pinning measurements, Schottky diodes

© 2023 The Authors. Advanced Materials Interfaces published by Wiley-VCH GmbH

consisting of an Ohmic and a Schottky contact were fabricated using shadow masks (Temicon GmbH, Dortmund) with a channel length of 10 µm and a contact width of 100 µm. The Ohmic contact was produced first by annealing a Ti/Al/Ti/Au (20/80/10/90 nm) metal stack deposited as above at 750 °C for 5 min in N_2 atmosphere (1.33 mbar pressure). The bare GaN samples were etched in concentrated (37%) HCl solution after annealing to reduce thermally grown oxide. The Schottky contacts were non-alloyed Ti/Au (20/80 nm), Cr/Pt/Au (50/20/30 nm), Au (50 nm), and Pt (50 nm) contacts deposited via electron-beam evaporation. For TLM measurements, 100 × 150 µm2 contact pads with spacings between 2 and 128 µm were defined using photolithography. J–V measurements were performed with a Keithley 2400 source meter.

X-Ray Photoelectron Spectroscopy: Two different experimental systems were used for XPS characterization. XPS spectra for native oxide overlayer characterization were acquired at a pass energy of 10 eV and a take-off angle of (90 ± 2) ° in a Kratos Axis Supra setup equipped with a monochromatic Al K_α X-ray source ($h\nu$ = 1486.7 eV) and operated at a base pressure of ≤ 9.2 × 10^{-9} mbar. The hemispherical analyzer was calibrated in situ using sputter-cleaned Ag, Au, and Cu standard samples. The instrumental broadening for this setup was determined to be 0.3 eV, as reported previously.[24] To clean the substrates for native oxide overlayer characterization, the surface adsorbate layer of air-exposed samples was removed using a previously reported selective sputtering procedure using Ar_{1000}^+ ion clusters that were tuned to preserve the chemical bonds of the GaN surface.[24]

XPS spectra for the determination of N to Ga atomic ratios were acquired at a pass energy of 20 eV and a take-off angle of 0° with an in-house built system (base pressure < 7 × 10^{-9} mbar) employing a Specs PHOIBOS 100 concentric hemispherical analyzer equipped with an MCD-5 detector and a Mg-K_α non-monochromatic X-ray source ($h\nu$ = 1253.6 eV). An instrumental broadening of 1.2 eV was determined by fitting the Au 4f core level spectrum of a freshly evaporated Au calibration sample.[55]

Surface Photovoltage Characterization: SPV measurements were performed using an in-house built CPD setup equipped with a commercial Kelvin probe and controller (Kelvin Probe S and Kelvin Control 07, Besocke Delta Phi GmbH). A collimated light-emitting diode (λ = 340 nm, ML340L4, Thorlabs) was used for illumination at an intensity of ≈35 mW cm^{-2}. A gold grid with a diameter of 3 mm and a work function of 4.8 eV was used as the reference electrode. During measurements, the chamber pressure was kept below 10^{-5} mbar. For relaxation, the GaN samples were held in the dark for 15 h before measurements, after which the remaining drift in the CPD signal (<10 mV h^{-1}) was small compared to the measured SPV. The measurement protocol was as follows: Sample load, 15 h evacuation, and relaxation, 1 h dark measurement, 1 h measurement under illumination, 2 h dark measurement. The SPV value was determined as the difference between the highest (negative) CPD value attained during the illumination period and the equilibrated CPD value directly before illumination. For good electric contact, Ti/Al/Ti/Au contacts were deposited outside of the CPD measurement area on the bare GaN samples and annealed at 750 °C in N_2 atmosphere for 5 min, while non-annealed Ti/Au contacts were deposited outside of the CPD measurement area of the ALD-treated GaN samples. For intensity-dependent SPV measurements, a variation in the illumination intensity over four orders of magnitude was realized by inserting appropriate neutral density filters into the LED beam path. For better comparison across intensities, the SPV value was consistently measured 40 s after switching on the illumination.

Supporting Information

Supporting Information is available from the Wiley Online Library or from the author.

Acknowledgements

This project has received funding from the European Research Council (ERC) under the European Union's Horizon 2020 research and innovation program (grant agreement No. 864234), the Deutsche Forschungsgemeinschaft (DFG, German Research Foundation) both under Germany´s Excellence Strategy – EXC 2089/1 – 390776260 (e-conversion) and through the TUM International Graduate School of Science and Engineering (IGSSE), and from TUM.Solar in the context of the Bavarian Collaborative Research Project Solar Technologies Go Hybrid (SolTech).

Conflict of Interest

The authors declare no conflict of interest.

Data Availability Statement

The data that support the findings of this study are available from the corresponding author upon reasonable request.

Keywords

atomic layer deposition, gallium nitride, interface engineering, ohmic contacts, plasma modification

Received: September 9, 2023
Revised: November 5, 2023
Published online: December 1, 2023

[1] C. Tong, in *Advanced Materials and Components for 5G and Beyond*, (Ed.: C. Tong), Springer Nature Switzerland, Cham, Switzerland **2022**, *327*, Ch. 2.
[2] E. A. Jones, F. F. Wang, D. Costinett, *IEEE J. Emerg. Sel. Top Power Electron* **2016**, *4*, 707.
[3] H. S. Wasisto, J. D. Prades, J. Gülink, A. Waag, *Appl. Phys. Rev.* **2019**, *6*, 041315.
[4] S. Huang, K. Wei, Z. Tang, S. Yang, C. Liu, L. Guo, B. Shen, J. Zhang, X. Kong, G. Liu, Y. Zheng, X. Liu, K. J. Chen, *J. Appl. Phys.* **2013**, *114*, 144509.
[5] D. Marcon, B. de Jaeger, S. Halder, N. Vranckx, G. Mannaert, M. van Hove, S. Decoutere, *IEEE Trans. Semicond. Manufact.* **2013**, *26*, 361.
[6] Z. H. Feng, Y. G. Zhou, S. J. Cai, K. M. Lau, *Appl. Phys. Lett.* **2004**, *85*, 5248.
[7] A. Firrincieli, B. de Jaeger, S. You, D. Wellekens, M. van Hove, S. Decoutere, *Jpn. J. Appl. Phys.* **2014**, *53*, 04EF01.
[8] J. Zhang, X. Kang, X. Wang, S. Huang, C. Chen, K. Wei, Y. Zheng, Q. Zhou, W. Chen, B. Zhang, X. Liu, *IEEE Electron Device Lett.* **2018**, *39*, 847.
[9] W. Shi, S. Huang, X. Wang, Q. Jiang, Y. Yao, L. Bi, Y. Li, K. Deng, J. Fan, H. Yin, K. Wei, Y. Li, J. Shi, H. Jiang, J. Li, X. Liu, *J. Semicond.* **2021**, *42*, 92801.
[10] S. Sedky, A. Witvrouw, H. Bender, K. Baert, *IEEE Trans. Electron. Devices* **2001**, *48*, 377.
[11] A. Motayed, R. Bathe, M. C. Wood, O. S. Diouf, R. D. Vispute, S. N. Mohammad, *J. Appl. Phys.* **2003**, *93*, 1087.
[12] E. Higurashi, T. Fukunaga, T. Suga, *IEEE J. Quantum Electron.* **2012**, *48*, 182.
[13] J. S. Foresi, T. D. Moustakas, *Appl. Phys. Lett.* **1993**, *62*, 2859.
[14] M. E. Lin, Z. Ma, F. Y. Huang, Z. F. Fan, L. H. Allen, H. Morkoç, *Appl. Phys. Lett.* **1994**, *64*, 1003.
[15] G. Greco, F. Iucolano, F. Roccaforte, *Appl. Surf. Sci.* **2016**, *383*, 324.
[16] S. Mohney, *Theoretical and Experimental Approach to Developing Improved Electrical Contacts to GaN*, Pennsylvania State University Park, Pennsylvania **1999**.

 © 2023 The Authors. Advanced Materials Interfaces published by Wiley-VCH GmbH

[17] J. D. Guo, C. I. Lin, M. S. Feng, F. M. Pan, G. C. Chi, C. T. Lee, *Appl. Phys. Lett.* **1996**, *68*, 235.
[18] M.-L. Lee, J.-K. Sheu, C. C. Hu, *Appl. Phys. Lett.* **2007**, *91*, 182106.
[19] T.-L. Wu, Y.-Y. Tseng, C.-F. Huang, Z.-S. Chen, C.-C. Lin, C.-J. Chung, P.-K. Huang, K.-H. Kao, *IEEE Workshop on Wide Bandgap Power Devices and Applications in Asia (WiPDA Asia)*, IEEE, Piscataway, NJ **2019**, pp. 1–4.
[20] M. Akazawa, T. Hasezaki, *Physica Status Solidi* **2018**, *255*, 1700382.
[21] J. Gong, K. Lu, J. Kim, T. Ng, D. Kim, J. Zhou, D. Liu, J. Kim, B. S. Ooi, Z. Ma, *Jpn. J. Appl. Phys.* **2022**, *61*, 011003.
[22] M. Esposto, S. Krishnamoorthy, D. N. Nath, S. Bajaj, T.-H. Hung, S. Rajan, *Appl. Phys. Lett.* **2011**, *99*, 133503.
[23] R. L. Puurunen, *J. Appl. Phys.* **2005**, *97*, 121301
[24] A. Henning, J. Bartl, A. Zeidler, S. Qian, O. Bienek, C.-M. Jiang, C. Paulus, B. Rieger, M. Stutzmann, I. Sharp, *Adv. Funct. Mater.* **2021**, *31*, 2101441.
[25] J. D. Hwang, G. H. Yang, C. C. Lin, S. J. Chang, *Solid-State Electron.* **2006**, *50*, 297.
[26] T. Maruyama, Y. Miyajima, S. H. Cho, K. Akimoto, H. Kato, *Phys. B* **1999**, *262*, 240.
[27] N. J. Shevchik, J. Tejeda, M. Cardona, *Phys. Rev. B* **1974**, *9*, 2627.
[28] B. R. Strohmeier, *Surf. Interface Anal.* **1990**, *15*, 51.
[29] J. B. Theeten, S. Gourrier, P. Friedel, M. Taillepied, D. Arnoult, D. Benarroche, *MRS Proc. Online Library* **2011**, *38*, 499.
[30] A. Y. Polyakov, I.-H. Lee, N. B. Smirnov, E. B. Yakimov, I. V. Shchemerov, A. V. Chernykh, A. I. Kochkova, A. A. Vasilev, A. S. Shiko, P. H. Carey, F. Ren, S. J. Pearton, *ECS J. Solid State Sci. Technol.* **2019**, *8*, P661.
[31] A. Venzie, A. Portoff, C. Fares, M. Stavola, W. B. Fowler, F. Ren, S. J. Pearton, *Appl. Phys. Lett.* **2021**, *119*, 062109.
[32] R. G. Wilson, S. J. Pearton, C. R. Abernathy, J. M. Zavada, *J. Vac. Sci. Technol. A: Vac., Surf. Films* **1995**, *13*, 719.
[33] Y. M. Strzhemechny, J. Nemergut, P. E. Smith, J. Bae, D. C. Look, L. J. Brillson, *J. Appl. Phys.* **2003**, *94*, 4256.
[34] E. Cartier, D. A. Buchanan, J. H. Stathis, D. J. DiMaria, *J. Non-Cryst. Solids* **1995**, *187*, 244.
[35] A. v. d. Heiden, M. Bornhöfft, J. Mayer, M. Martin, *Phys. Chem. Chem. Phys. PCCP* **2019**, *21*, 4268.
[36] J. Uhlendorf, Z. Galazka, H. Schmidt, *Appl. Phys. Lett.* **2021**, *119*, 242106.
[37] T. Nabatame, T. Yasuda, M. Nishizawa, M. Ikeda, T. Horikawa, A. Toriumi, *Jpn. J. Appl. Phys.* **2003**, *42*, 7205.
[38] R. Nakamura, T. Toda, S. Tsukui, M. Tane, M. Ishimaru, T. Suzuki, H. Nakajima, *J. Appl. Phys.* **2014**, *116*, 033504.
[39] P. Laukkanen, M. P. J. Punkkinen, M. Kuzmin, K. Kokko, J. Lång, R. M. Wallace, *Appl. Phys. Rev.* **2021**, *8*, 011309.
[40] Z. Xie, Y. Sui, J. Buckeridge, C. R. A. Catlow, T. W. Keal, P. Sherwood, A. Walsh, M. R. Farrow, D. O. Scanlon, S. M. Woodley, A. A. Sokol, *J. Phys. D: Appl. Phys.* **2019**, *52*, 335104.
[41] B. S. Eller, J. Yang, R. J. Nemanich, *J. Electron. Mater.* **2014**, *43*, 4560.
[42] M. Foussekis, A. A. Baski, M. A. Reshchikov, *J. Vac. Sci. Technol. B Nanotechnol. Microelectron. Mater., Process.* **2011**, *29*, 41205.
[43] D. R. Jennison, P. A. Schultz, J. P. Sullivan, *Phys. Rev. B* **2004**, *69*, 041405(R).
[44] O. A. Dicks, J. Cottom, A. L. Shluger, V. V. Afanas'ev, *Nanotechnology* **2019**, *30*, 205201.
[45] M. Grundmann, *The Physics of Semiconductors*, Springer International Publishing, Berlin, Germany **2016**.
[46] R. Adari, D. Banerjee, S. Ganguly, D. Saha, *Thin Solid Films* **2014**, *550*, 564.
[47] H. Hasegawa, Y. Koyama, T. Hashizume, *Jpn. J. Appl. Phys.* **1999**, *38*, 2634.
[48] U. Karrer, *Schottky-Dioden auf Galliumnitrid. Eigenschaften und Anwendungen in der Sensorik*, Walter Schottky Institute, Garching bei München, Germany **2002**.
[49] J. Tersoff, *Phys. Rev. Lett.* **1984**, *52*, 465.
[50] S. M. Sze, K. K. Ng, *Physics of Semiconductor Devices*, John Wiley & Sons, Inc, New York **2007**.
[51] S. Chand, J. Kumar, *J. Appl. Phys.* **1997**, *82*, 5005.
[52] O. Ambacher, *J. Phys. D: Appl. Phys.* **1998**, *31*, 2653.
[53] X. Qin, H. Dong, B. Brennan, A. Azacatl, J. Kim, R. M. Wallace, *Appl. Phys. Lett.* **2013**, *103*, 221604.
[54] S. Peters, T. Schmidtling, T. Trepk, U. W. Pohl, J.-T. Zettler, W. Richter, *J. Appl. Phys.* **2000**, *88*, 4085.
[55] J. D. Bartl, P. Scarbolo, D. Brandalise, M. Stutzmann, M. Tornow, L. Selmi, A. Cattani-Scholz, *Langmuir* **2019**, *35*, 3272.

© 2023 The Authors. Advanced Materials Interfaces published by Wiley-VCH GmbH